# Surface Diffusion and Dendrite Formation in Alkali-Metal Anodes

Mathus Jirapunyawong
Supervised by Prof. Kari Laasonen

Metallic lithium batteries are prone to dendrite formation—needle-like metallic protrusions that develop during repeated charge–discharge cycling. These structures arise from non-uniform adatom deposition and growth on the anode surface. Once metallic Li atoms are electrochemically reduced and deposited, their ability to migrate across the surface determines whether the electrode evolves toward a smooth morphology (high adatom mobility) or develops localized protrusions (low mobility). Consequently, surface diffusion barriers are directly correlated with dendrite risk: high diffusion barriers restrict adatom motion and promote rough, uneven deposition, whereas low barriers facilitate surface self-smoothing and suppress dendrite initiation.

This study systematically evaluates surface diffusion barriers for several alkali-metal anodes—Li, Na, and K—across the most common low-index crystal facets. In addition, the influence of surface imperfections is examined by modeling step-edge diffusion on Li(110), representing a more realistic defect-containing surface. All calculations are performed using Density Functional Theory (DFT) combined with the Nudged Elastic Band (NEB) method to resolve minimum-energy pathways and quantify activation barriers for adatom migration.

## Adatom Diffusion on the (110) Surface

The bcc(110) surface was selected as the primary comparison facet for this study because it is (i) the most open and reactive low-index surface of bcc metals, (ii) widely used as a model system for alkali-metal surface science, and (iii) representative of the rough and stepped regions on which dendrites preferentially nucleate. The full workflow and scripts used for the diffusion calculations are available at:

https://github.com/Tew12345678910/DFT-Surface-Diffusion-and-Dendrite-Formation/blob/main/multi_material_neb_pipeline_restartable_time.ipynb

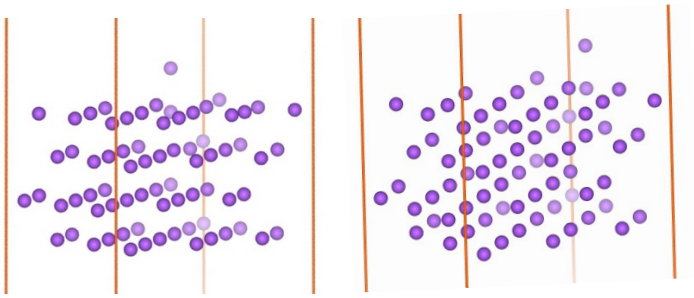

Li(110) diffusion is shown above, where the adatom migrates from the initial adsorption site (left) to the adjacent final site (right).

Surface diffusion barriers were computed using the Nudged Elastic Band (NEB) method implemented in the Atomic Simulation Environment (ASE), with GPAW serving as the Density Functional Theory (DFT) engine. Metal slabs (Li, Na on bcc(110)) were constructed using ASE's surface() function, consisting of four atomic layers and a 3×3×1 supercell. A vacuum region of 10 Å was added along the surface normal. To approximate bulk constraints, the bottom 50% of the atoms were fixed using FixAtoms.

Two neighboring adsorption sites on the top surface were automatically detected and used as the initial and final positions for the diffusing adatom. For each configuration, a Li or Na adatom was placed 2.0 Å above the corresponding surface site.

All calculations employed the PBE exchange–correlation functional, a plane-wave basis with a 200 eV cutoff, and a 2×2×1 Monkhorst–Pack k-point mesh. Electronic convergence thresholds were set to $5\times10^{-6}$ eV for the eigenstates and $10^{-4}$ for the electron density. Initial and final states were relaxed via the BFGS optimizer until atomic forces were below 0.05 eV $Å^{-1}$.

Minimum energy paths were determined using climbing-image NEB with five intermediate images between the endpoints. The FIRE optimizer was used for the NEB relaxation with a maximum force threshold of 0.10 eV $Å^{-1}$. Diffusion barriers were obtained as the energy difference between the highest-energy NEB image (transition state) and the lower-energy endpoint.

To improve robustness during long NEB calculations, a status-tracking workflow (status.json) was implemented to allow checkpoint–restart capability. This prevented loss of progress in the event of partial runs or interruptions.

Despite using the checkpoint system, repeated failures occurred on the kvantti2 cluster due to unpredictable Python environment terminations. While RAM usage typically remained below the 4 GB limit, brief spikes in memory consumption occasionally caused kernel crashes, preventing the completion of NEB calculations even after restarts. As a solution, GPAW was installed locally on my personal MacBook M2 (16 GB RAM), and the workflow was executed using VS Code. The higher available memory allowed all calculations to run smoothly, with overall

performance slightly exceeding that of kvantti2. The final results reported in this work were therefore obtained from the local environment.

**Lithium (Li bcc-110)**

Lithium exhibits the highest diffusion barrier among the three alkali metals examined. The plane-wave NEB calculations yield a barrier of **0.0387 eV**, in excellent agreement with previously reported values for Li adatom diffusion on Li(110), which typically fall in the range of 0.02–0.05 eV. The NEB pathway shows a pronounced corrugation in the surface potential, indicating that Li adatoms encounter relatively deep adsorption wells and substantial resistance to lateral motion. This behavior reflects intrinsic material properties: lithium's small atomic radius, comparatively localized electron density, and strong adatom–substrate interaction collectively enhance the energy contrast between neighboring sites. As a result, adatoms tend to remain confined near their point of deposition rather than migrating extensively across the surface. The reduced mobility provides a mechanistic explanation for the well-documented tendency of Li metal to form dendritic deposits; with limited surface diffusion, initial height variations cannot be smoothed out, and surface asperities are amplified during cycling.

**Sodium (Na bcc-110)**

Sodium displays an exceptionally low diffusion barrier on the Na(110) surface, with the plane-wave NEB calculation returning a value effectively equal to zero within the limits of DFT numerical accuracy. The surface energy landscape is almost flat, allowing Na adatoms to move nearly freely across the terrace. Such behavior aligns with experimental observations that Na metal anodes exhibit substantially less severe dendritic growth relative to Li. The high surface mobility enables Na deposits to redistribute rapidly, promoting the formation of smooth, uniform layers rather than localized protrusions. Although the computed value approaches the threshold of resolution imposed by the chosen cutoff energy and k-point sampling, the physical picture remains unambiguous: sodium adatoms experience minimal energetic resistance to motion on Na(110), and terrace diffusion is effectively barrierless.

**Potassium (K bcc-110)**

The diffusion behavior of potassium proved more challenging to evaluate in plane-wave mode due to the material's large lattice constant and highly diffuse valence electron cloud, which increased computational cost and led to repeated convergence difficulties. To overcome these obstacles, the calculation was performed using the LCAO basis set in GPAW, which considerably reduces computational requirements by expanding the wavefunction in localized atomic orbitals rather than plane waves. Because PW and LCAO approaches differ

fundamentally, calibration calculations were performed for Li and Na in both modes to quantify systematic discrepancies.

Using identical slab geometries, supercells, and vacuum conditions, the LCAO calculations (employing Γ-point sampling and the standard DZP basis) produced diffusion barriers of **0.0135 eV** for Li, **0.0006 eV** for Na, and **0.0254 eV** for K. As expected, the LCAO method underestimates the Li barrier relative to PW due to unavoidable error that arises when the basis set is too limited while the Na result remains consistent with the near-zero barrier obtained previously. The K diffusion barrier of 0.0254 eV is physically reasonable given potassium's large atomic radius, soft electron cloud, and weak adatom–surface interactions. These properties collectively result in shallow potential energy corrugation and very rapid surface diffusion. This high intrinsic mobility helps explain why potassium metal is experimentally observed to grow in large, smooth grains rather than sharp whiskers, and why dendrite formation in K metal anodes is significantly less problematic than in lithium. Scripts used for the LACO diffusion calculations are available at:

https://github.com/Tew12345678910/DFT-Surface-Diffusion-and-Dendrite-Formation/blob/main/multi_material_neb_pipeline_LCAO_restartable_time.ipynb

| Metal | Plane Wave | LCAO |
|---|---|---|
| Li | 0.0387 | 0.0135 |
| Na | 0.0000 | 0.0006 |
| K | - | 0.0254 |

Summary of Diffusion Barriers (PW and LCAO)

## Effect of Lattice Structure on the Diffusion Barrier

To investigate how crystallographic orientation influences lithium adatom mobility, diffusion barriers were calculated for the low-index BCC Li surfaces: Li(110), Li(100), and Li(111). Previous discussion highlighted why Li(110) is commonly selected as the standard reference surface for benchmarking diffusion calculations—it is the most stable and best-behaved surface in terms of energy convergence, making it suitable for NEB studies. To validate this assumption and to test whether lattice geometry meaningfully alters Li adatom mobility, identical PW-NEB procedures were applied to Li(100) and Li(111). Scripts used for the diffusion calculations for different crystal strcture are available at:

https://github.com/Tew12345678910/DFT-Surface-Diffusion-and-Dendrite-Formation/blob/main/crystal_structure_neb.ipynb

The NEB calculations in plane-wave mode yielded the following barrier energies:

| Surface | Barrier (eV) |
|---|---|
| Li(110) | 0.0387 |
| Li(100) | 0.0008 |
| Li(111) | 0.0001 |

Li(110) shows a well-defined and physically meaningful diffusion barrier. In contrast, both Li(100) and Li(111) exhibit barriers that are nearly zero, suggesting a very smooth potential landscape for adatom motion. However, barriers below ~1 meV fall below the numerical resolution of typical DFT and NEB calculations. Therefore, the extremely small barriers obtained for Li(100) and Li(111) require careful interpretation.

To evaluate whether the unusual behaviour of Li(100) and Li(111) was caused by insufficient computational accuracy, convergence tests were performed using plane-wave cutoffs of 300–600 eV and k-point meshes of 2×2×1, 3×3×1, and 4×4×1. Convergence errors were evaluated relative to the most converged reference (600 eV, 4×4×1).

The script loads pre-relaxed initial adatom structures from previous NEB calculations. It then creates a GPAW calculator with the specified plane-wave cutoff and k-point mesh, using tight convergence criteria (eigenstates: $5\times10^{-6}$, density: $1\times10^{-4}$). The k-points are defined as (k, k, 1), with the z-direction reduced to reflect the slab geometry. The scripts can be found at :

https://github.com/Tew12345678910/DFT-Surface-Diffusion-and-Dendrite-Formation/blob/main/li_kpoint_cutoff_convergence.ipynb

**Convergence Errors (meV)**

Li 110

| eCut, k (k x k x 1) | 2 | 3 | 4 |
|---|---|---|---|
| 300 | 470.829 | 62.552 | 16.254 |
| 400 | 463.360 | 55.458 | 8.813 |
| 500 | 455.719 | 47.610 | 1.191 |
| 600 | 454.536 | 46.354 | 0.000 |

Li111

| eCut, k (k x k x 1) | 2 | 3 | 4 |
|---|---|---|---|
| 300 | -89.563 | -56.694 | 15.297 |
| 400 | -96.488 | -63.598 | 8.363 |
| 500 | -103.688 | -70.739 | 1.163 |
| 600 | -104.848 | -71.894 | 0.000 |

Li100

| eCut, k (k x k x 1) | 2 | 3 | 4 |
|---|---|---|---|
| 300 | 422.812 | 88.150 | 15.952 |
| 400 | 415.533 | 80.900 | 8.726 |
| 500 | 408.037 | 73.369 | 1.175 |
| 600 | 406.900 | 72.168 | 0.000 |

Li(110) showed large absolute energy errors at coarse k-meshes (≈450 meV at 2×2×1), but these errors decreased systematically with increasing k-point density. Li(100) exhibited a similar pattern, with errors of ≈400 meV at 2×2×1 and much smaller deviations at 4×4×1, indicating broadly predictable convergence behaviour. In contrast, Li(111) displayed unusual non-monotonic convergence, including negative errors, which is a signature of its intrinsic metastability. Li(111) is not a natural cleavage plane of BCC lithium and therefore has the highest surface energy among the studied orientations. Upon relaxation, it undergoes significant reconstruction, producing a shallow and complex potential-energy landscape that is highly sensitive to slab thickness, k-point sampling, and numerical settings. Coarse k-meshes may artificially stabilise certain reconstructed surface configurations, resulting in deceptively low or even negative convergence errors. This metastability also leads to poorly defined adsorption sites and transition states, causing the computed diffusion barrier (0.0001 eV) to fall below the numerical noise level. Consequently, the Li(111) barrier reflects numerical artefacts rather than a physically meaningful energetic pathway.

A key finding from these analyses is that the magnitude of the total-energy convergence error does not correlate with the reliability of the diffusion barrier. For example, Li(100) shows smaller total-energy errors than Li(110), yet produces an unreliable diffusion barrier. This occurs because diffusion barriers depend on the curvature of the potential energy surface (PES), not on the absolute accuracy of total energies. Li(110) is the lowest-energy and most stable BCC Li surface; it undergoes minimal reconstruction and exhibits a well-defined PES with a clear adsorption minimum and saddle point. This produces a barrier of 0.0387 eV that lies comfortably above the SCF and NEB numerical noise levels, making it quantitatively reliable despite the relatively large absolute energy errors at coarse k-meshes.

In contrast, the PES of Li(100) is intrinsically extremely flat, resulting in a computed barrier of just 0.0008 eV. The energy difference between the adsorption site and the transition state is <1 meV—smaller than typical SCF fluctuations, NEB spring-force uncertainties, and far below thermal energy at room temperature (kBT ≈ 0.025 eV). Thus, even though Li(100) converges reasonably in total energy, NEB cannot meaningfully resolve such a small barrier. The result reflects a combination of physical flatness and numerical noise, rather than a trustworthy diffusion energy.

Li(111) behaves similarly but more severely: its metastability, reconstruction tendencies, and highly sensitive electronic surface states produce a barrier (0.0001 eV) that is effectively indistinguishable from zero and entirely dominated by numerical artefacts. As with Li(100), the barrier suggests qualitatively fast diffusion but cannot be interpreted quantitatively.

## Step-Edge Diffusion of Li Adatoms on the Li(110) Surface

Lithium metal anodes exhibit highly anisotropic surface diffusion behavior, and step defects are known to significantly influence nucleation processes and dendrite growth. Compared to ideal terraces, atomic step edges modify the local coordination environment and can either increase or decrease migration barriers depending on the direction of motion.

To evaluate the energetics of Li adatom descent across a monoatomic step on Li(110), that the step have been created. And since the supercell size is increase significately (from 4 atomic layers and a 3×3×1 supercell to 4×4×6 supercell) the PW mode is not feasible thus LCAO mode is use instead

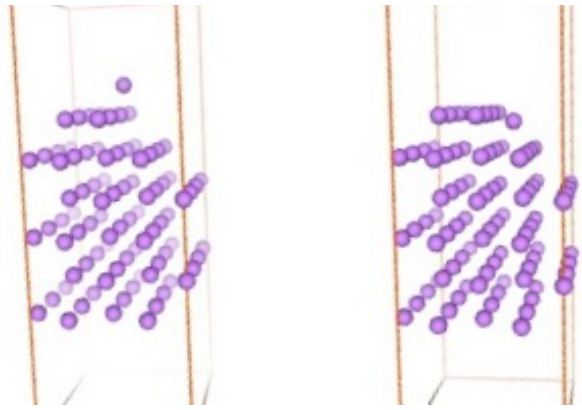

Li adatom positioned at the step edge (right) and the corresponding final state after descending to the lower terrace (left).

A Li(110) step-edge slab was constructed using ASE's bcc110() function with a 4×4×6 supercell (nx, ny, nz) and a lattice constant of 3.49 Å. A vacuum layer of 8.0 Å was added perpendicular to the surface. A monoatomic step was created by removing atoms from the topmost layer on one half of the slab (y < y_cut), producing distinct upper and lower terraces. The bottom 50% of slab atoms were fixed to simulate bulk behavior.

The adatom was placed 2.0 Å above the surface, with initial and final positions on the upper and lower terraces respectively. The edge_fraction parameter (0.3) positioned the adatom closer to the step edge rather than at the terrace center, ensuring the diffusion path crossed the step.

Calculations employed the PBE exchange-correlation functional with LCAO (Linear Combination of Atomic Orbitals) basis set mode, a 2×2×1 k-point mesh, and Fermi-Dirac smearing with a width of 0.1 eV. Initial and final configurations were relaxed using the BFGS optimizer until forces converged below 0.05 eV/Å.

The minimum energy path for step-edge descent was determined using the climbing-image NEB method with 5 total images (including endpoints). The FIRE optimizer was employed with a force convergence threshold of 0.10 eV/Å and a maximum of 300 optimization steps. The step-edge diffusion barrier was extracted as the energy difference between the transition state and the lower-energy endpoint. Scripts used for the step diffusion calculations are available at:

https://github.com/Tew12345678910/DFT-Surface-Diffusion-and-Dendrite-Formation/blob/main/step_v4/Li110_step_edge_neb_restartable_json_visual.ipynb

The calculated step-descent barrier of **0.766 eV** is consistent with the general observation that descending across a step edge is far more difficult than migrating laterally on a flat terrace. For comparison, the terrace diffusion barrier on Li(110) is only **0.0387 eV**, meaning that step descent is more than an order of magnitude more kinetically hindered—even when computed using the LCAO method. This highlights the strong asymmetry between in-plane and cross-step atomic motion.

Such a high barrier implies that monoatomic step edges on Li(110) function as major kinetic bottlenecks. Under ambient conditions, the probability of an adatom crossing a step is extremely low, leading to significantly reduced hopping rates relative to terrace diffusion. As a consequence, Li adatoms tend to accumulate on upper terraces rather than descend to lower ones. This behaviour aligns with established growth models: when step crossing is inhibited, adatoms cluster on ledges, promoting multilayer island formation, surface roughening, and ultimately the development of vertical protrusions.

From the perspective of lithium-metal anode stability, these results suggest that step edges may be critical sites for non-uniform growth during electrodeposition. Because adatoms cannot efficiently descend steps, they preferentially aggregate on elevated regions, which can act as seeds for uneven deposition and potentially evolve into dendritic structures. The energetics

presented here therefore provide mechanistic insight into how stepped Li surfaces can contribute to morphological instability even without strong electrochemical driving forces.